Supporting Information

Magnetic Force Fields of Isolated Small Nanoparticles Clusters

C. Iacovita [1,2], J. Hurst [3], G. Manfredi [1], P. A. Hervieux [1], B. Donnio [1], J. L. Gallani [1], M. V. Rastei [1 *]

[1] *Institut de Physique et Chimie des Matériaux de Strasbourg, CNRS, Université de Strasbourg,*

F-67034 Strasbourg, France

[2] *Department of Pharmaceutical Physics-Biophysics, Faculty of Pharmacy, "Iuliu Hatieganu"*

University of Medicine and Pharmacy, Pasteur 6, 400349 Cluj-Napoca, Romania

[3] *Department of Physics and Astronomy, Uppsala University, P. O. Box 516, SE-75120 Uppsala, Sweden*

e-mail: mircea.rastei@ipcms.unistra.fr

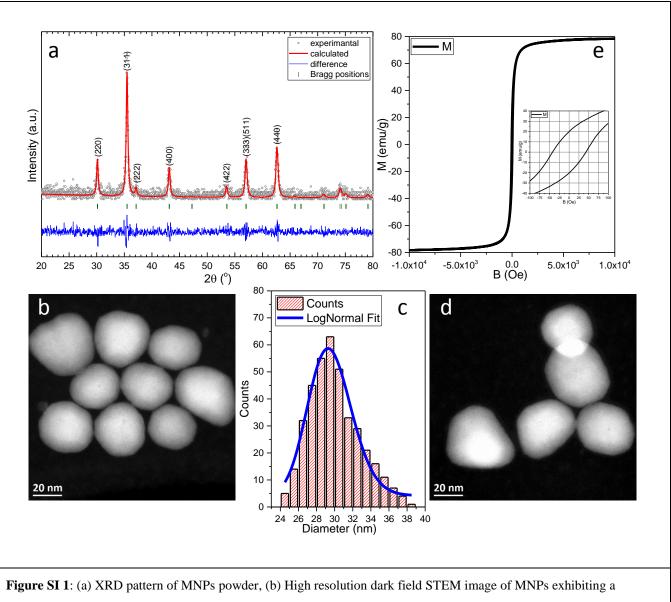**Sup. Mat. 1: Synthesis of magnetic nanoparticles**

All the reagents employed in this study were purchased from Sigma – Aldrich, of analytical grade and used without any further purification. The MNPs were prepared by high temperature decomposition of iron(III) acetylacetonate in organic solvent [1], that enable to produce highly crystalline MNPs with a wide range of monodispersed sizes distribution. In a general synthetic procedure for the preparation of iron oxide magnetic nanoparticles (MNPs), 1 mmol of iron(III) acetylacetonate (0.35 g) were dissolved in a mixture of 1.9 ml of oleic acid and 2 ml of octylether. The solution was stirred thoroughly at room temperature for 30 minutes and then transferred in a 10 ml round-bottom flask, being part of a home-made stainless steel reaction vessel. Prior to sealing the reaction vessel using a Teflon gasket and five screws, the solution has been degassed by exposure to a flux of nitrogen gas for 5 minutes. The reaction vessel has been introduced into an oven (Naberthem) equipped with a temperature controller (JUMO dTron 316) that allow programing the heating. The solution was firstly heated from room temperature to 200°C with a constant heating rate of 4°C/min. After 2 h at 200°C, the solution was further heated up to 300°C, using the same heating rate of 4°C/min and kept at this temperature for an additional 1 h. The reaction vessel was let to cool to room temperature, the excess liquid was discharged and the obtained black precipitate was washed with ethanol by means of multiple ultasonication/magnetic separation cycles, in order to remove the excess of ligands and unreacted precursors. Finally, the black precipitate was dispersed and kept in 10 mL of chloroform.

Sup. Mat. 2: Structural and magnetic characterization of magnetic nanoparticles

X-ray diffraction (XRD) measurements were carried out on powder sample, obtained by evaporating the solvent using a rotary evaporator (Heidolph), at room temperature on a Bruker D8 Advance diffractometer (Bruker-AXS GmbH, Karlsruhe, Germany) using Cu Kα radiation. The XRD pattern (figure SI1) clearly reveals the existence of a pure inverse spinel crystalline structure, while the position and the relative intensities of all diffraction peaks ascribed to magnetite Fe_3O_4 (PDF number: 88-0315 [2]). No FeO or Fe_2O_3 peaks were found in the XRD pattern, indicating that the MNPs consist of pure magnetite Fe_3O_4. The black color of the powder further confirms that MNPs is of pure magnetite phase. The corresponding lattice parameter (a = 8.381 Å), calculated using the FullProf software

(http://www.crystalimpact.com/match/download.htm), is were very close to that of bulk magnetite (a = 8.375 Å). The mean crystalline size of Fe_3O_4 MNPs, calculated from the (220), (311), (400) diffraction peaks using Debye-Scherrer's formula was 28.85 nm [3].

Transmission Electron Microscopy (TEM) analysis was carried out on a JEOL-2100F microscope working at 200 kV. For TEM examination, 5 μL drop of MNPs suspension in chloroform was deposited on carbon-coated copper grids and left to dry under ambient air. The Fe_3O_4 MNPs display a spherical shape and sharp size distribution with a mean diameter of 29.5 nm (figure SI1) in good agreement with the estimation from XRD data.

Magnetic hysteresis loop, was performed on an Alternative Gradient Field Magnetometer (AGFM) under magnetic fields up to 1T at room temperature. Multiple drops of Fe_3O_4 MNPs dispersed in chloroform have been deposited on a square silicon plate (5 x 5 mm^2). Upon the complete evaporation of the entire solvent, the sample has been weighted with a five digits electronic balance, thus determining the mass of magnetic powder deposited of silicon plate. The organic coating of MNPs was neglected since a mass loss of 2% has been recorded in the temperature interval 25-700°C according to TGA-SDTA measurement. Finally, the magnetic powder was covered by a thin layer of super-glue to ensure their stability on the silicon substrate during the AGFM measurements. As depicted in figure SI1, the magnetization curve reveals that the Fe_3O_4 MNPs are in a ferromagnetic state at room temperature, with a coercive field of about 40 Oe and a remanence magnetization of 20 emu/g. The magnetization increases rapidly up to 75 emu/g when the external field is swept to 0.25 T (2500 Oe) and then saturates slowly to 79 emu/g for external field of 1 T (10000 Oe). The saturation magnetization of 79 emu/g is slightly smaller than the bulk saturation magnetization of magnetite at room temperature (84 emu/g), indicating an almost perfect ferromagnetic order throughout the whole MNPs, as previously observed for similar MNPs synthesized by the thermal decomposition method.

Figure SI 1: (a) XRD pattern of MNPs powder, (b) High resolution dark field STEM image of MNPs exhibiting a spherical shape, (c) Experimental histogram together with the log-normal fit, (d) High resolution dark field STEM image of MNPs showing the superposition of two MNPs and (e) Magnetic hysteresis loop of MNPs; the inset is a zoom-in the hysteresis loop.

Sup. Mat. 3: AFM and MFM characterization of magnetic nanoparticles

AFM and MFM experiments have been performed under open environment and ambient conditions using a standard commercial ICON-AFM QNM-PeakForce apparatus from Bruker. The topographic AFM images have been acquired in tapping mode, while a dynamic tapping/lift mode was employed for the MFM imaging. The MFM tips employed in this research are commercially available hard magnetic coating silicon tips (NanoSensors[TM] – code: PPP-LM-MFMR-20). The nominal spring constant of the cantilever is $k = 2.8\ N/m$, while the resonance quality factor is $Q = 660$. The coercivity of the hard magnetic coating is about 250 Oe and the remanence magnetization is about 150 emu/cm^{3}. All images were collected with at 1.5 lines/s and with a resolution of 256x256 pixels. The amplitude set point of the tip-cantilever oscillations was set in between 12-18 nm.
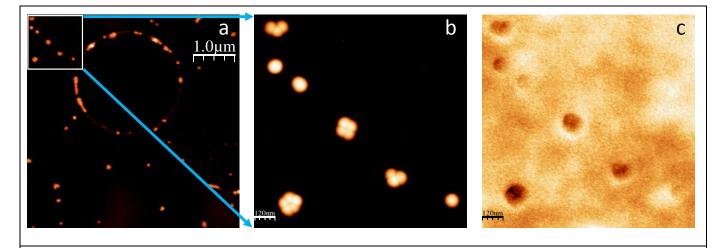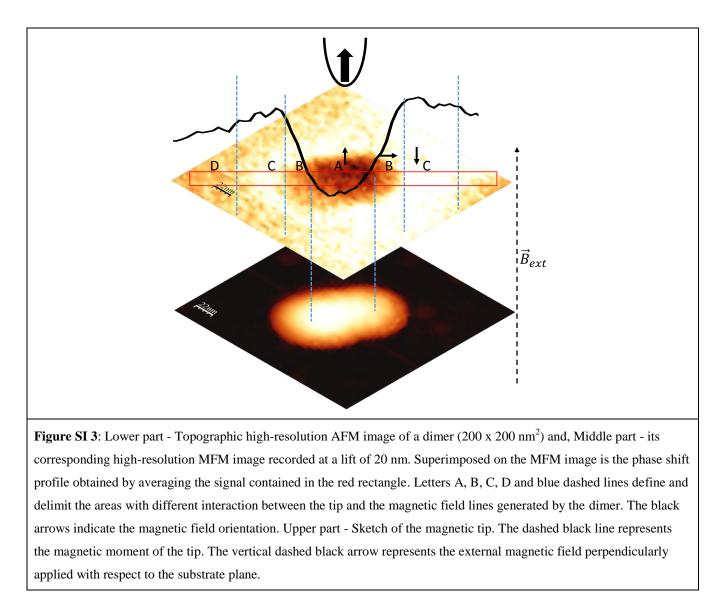

Figure SI 2: (a) Large scale topographic AFM image of MNPs (4.5 x 4.5 μm^2); (b) Topographic AFM image of single nanoparticles oligomers (1.1 x 1.1 μm^2) and (c) the corresponding MFM image recorded at a lift of 20 nm above the substrate.

One drop of dilute MNPs suspension in chloroform has been deposited onto a carbon-coated copper grid and dried at room temperature. The sample has been positioned on a cube shape permanent magnet capable of generating nearby a magnetic field strength of 0.5 T in vertical (Oz) direction. This means that the MFM measurements were performed with both the tip and the MNPs being in magnetically saturation state. Large topographic AFM image show MNPs self-assembled in the so called coffee-rings (figure SI 2a), as a consequence of subsequent evaporation of both chloroform and water (a small fraction is contained in chloroform). Among individual MNPs, different others 2D associations of single

MNPs can be found, as dimers, trimers, tetramers, pentamers, chains etc., denominated single nanoparticle oligomers (figure SI 2a and b). In the presence of the externally applied magnetic field, the magnetic moments of both tip and oligomers are aligned parallel and thus a strong dark contrast due to attractive dipole-dipole interaction is recorded over the whole range of oligomers (figure SI 2c).

Figure SI 3: Lower part - Topographic high-resolution AFM image of a dimer (200 x 200 nm^2) and, Middle part - its corresponding high-resolution MFM image recorded at a lift of 20 nm. Superimposed on the MFM image is the phase shift profile obtained by averaging the signal contained in the red rectangle. Letters A, B, C, D and blue dashed lines define and delimit the areas with different interaction between the tip and the magnetic field lines generated by the dimer. The black arrows indicate the magnetic field orientation. Upper part - Sketch of the magnetic tip. The dashed black line represents the magnetic moment of the tip. The vertical dashed black arrow represents the external magnetic field perpendicularly applied with respect to the substrate plane.

The high-resolution MFM image recorded on a dimeric cluster clearly visualizes the generated magnetic field lines under the applied external magnetic field. Right over the cluster, the magnetic contrast is dark and uniformly distributed over its surface area (A area in figure SI3), corresponding to an attractive dipole-dipole interaction due to the parallel orientation of the magnetic field lines with the tip's magnetic moment. In the phase shift profile this area appears as a depression. Note that due to the

convolution of tip-sample interactions the cluster appears wider in the topographic AFM image. Around the cluster two annular areas can be distinguished. In the B area, the dark contrast loses in intensity and turns into a bright one. The orientation of the magnetic field lines turns, changing the attractive dipole-dipole interaction to a repulsive one. The phase shift passes from negative values to positive ones. The bright contrast reaches a maximum and then decreases in intensity as going away from the cluster (C area in figure SI3). In the C area, the magnetic field lines are antiparallel oriented with the tip's magnetic moment giving rise to repulsive dipole-dipole interaction. The phase shift reaches maximum positive values and decreases gradually to zero far away from cluster (area D in figure SI3). The D area represents the zero level taken as reference in the determination of each value of the phase shift presented in figures 2, 3 and 4 from the main text. Quantitatively, each value of the phase shift is an average over a square area (25 x 25 nm^2) situated in the middle of the depression (A area).

Sup. Mat. 4: Magnetic tip calibration within point probe two-dipole model

The obtained value of the saturation magnetization (M_s) allows the calculation of the magnetic moment of spherical single MNPs with a given diameter d using the relation:

$$m_{MNP} = M_S V = M_S \frac{\pi d^3}{6} \ (1)$$

Under an external magnetic field of 0,5 T the $M_s = 77 \ emu/g$. Since the density of Fe$_3$O$_4$ is $\rho_{Fe_3O_4} = 5,15 \frac{g}{cm^3}$, 1 g of MNPs occupies a volume of $0.2 \ cm^3$. Thus the saturation magnetization of Fe$_3$O$_4$ MNPs become $M_s = \frac{77}{2} x \ 10^{10} \ A/m$ at room temperature. By applying the relation (1), the magnetic moments of certain spherical Fe$_3$O$_4$ MNPs, with well-known diameters, can be easily calculated as shown in Table SI 1.

Generally, in the literature, the magnetic interaction between MNPs and the magnetic tip has been exploited, in a very simple manner, in terms of dipole-dipole approximation of two-dipole model. In this very simple model, one of the dipole is located in the middle of the MNPs (considered as sphere), whereas the other is virtually positioned within the tip at certain distance in respect to the tip apex (figure SI 4.).

The magnetic phase shift within this model can be obtained as (see ref 45 in main text for instance):

$$\Delta \varphi = -\frac{180}{\pi} \frac{Q}{k} \frac{\mu_0}{\pi} m_{MNPS} m_{tip} \frac{6}{(z+t)^5} \ (2)$$

where, Q and k are the quality factor (660) and the spring constant of the used cantilever (2.8 N/m), μ_0 is the permeability of the free space (4π x $10^{-7} \ H/m$), z is the experimental lift height and $t = \frac{d}{2} + c_s + A_{sp} + \delta_{tip}$; d is the diameter of the MNPs, c_s the thickness of the possible non-magnetic coating of MNPs (is considered zero in our case), A_{sp} is the amplitude set-point (17-18 nm in our case) and δ_{tip} is the virtual position, in respect to the tip apex, of the effective magnetic dipole of the tip. The phase shift expressed with relation (2) can be reduced to:

$$\Delta \varphi = \frac{a}{(z+t)^5} \ (3)$$

$$where \ a = -6 \frac{180}{\pi} \frac{Q}{k} \frac{\mu_0}{\pi} m_{MNPS} m_{tip} = -3,25 \ x \ 10^{-2} \ m_{MNPS} \ m_{tip} \ (4)$$

Since the m_{MNPs} are known with a good precision, the fitting of $\Delta\varphi = f(z)$ curves recorded for six single MNPs with the equation (3), allow us to determine the m_{tip} and its virtual location within the tip volume δ_{tip} (Table SI 1).

Table SI 1: Diameters and the corresponding calculated magnetic moments of six spherical MNPs; fitting parameters of $\Delta\varphi = f(z)$ curves within dipole-dipole model; and the magnetic moment of the tip involved in collecting the signal as well as its virtual location within the tip volume.

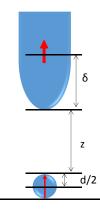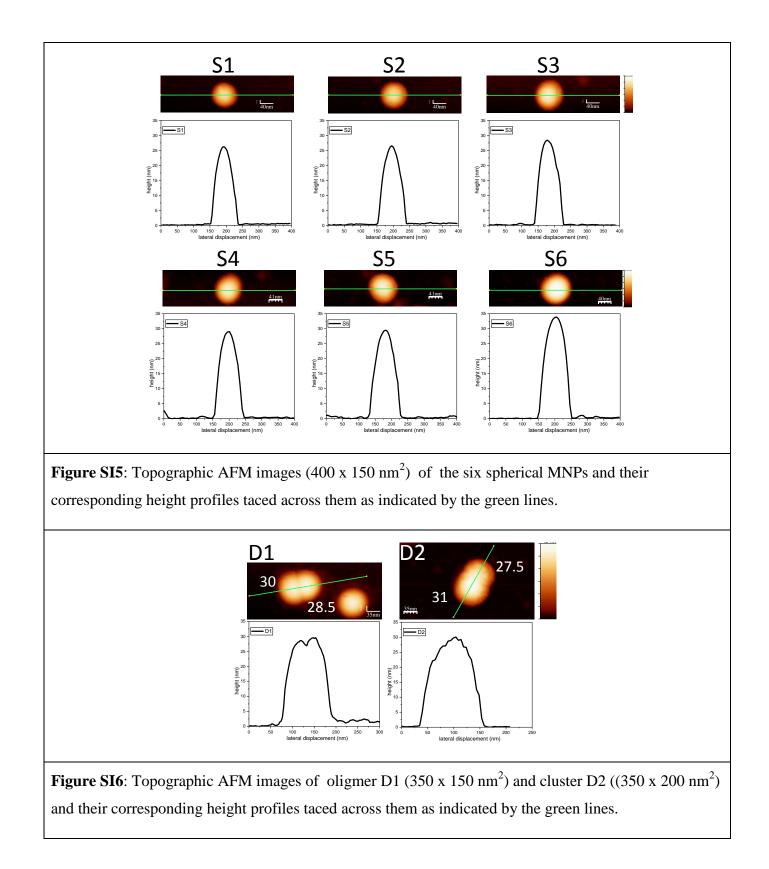| MNPs	Diameter of MNPs (nm)	Theoretical magnetic moment of MNPs (Am^2)	Parameter a from fit (m^5)	Parameter t from fit (m)	Experimental magnetic moment of the tip (Am^2)	Virtual location within the tip volume (nm)
S1	26	3.54 x 10^{-18}	-1.554 x 10^{-36}	86.85 x 10^{-9}	1.35 x 10^{-17}	56
S2	26.5	3.75 x 10^{-18}	-1.908 x 10^{-36}	89.85 x 10^{-9}	1.57 x 10^{-17}	59
S3	28.5	4.66 x 10^{-18}	-2.623 x 10^{-36}	95.04 x 10^{-9}	1.73 x 10^{-17}	63
S4	29	4.91 x 10^{-18}	-3.065 x 10^{-36}	99.78 x 10^{-9}	1.92 x 10^{-17}	67
S5	30	5.44 x 10^{-18}	-3.801 x 10^{-36}	101.93 x 10^{-9}	2.15 x 10^{-17}	69
S6	34	7.92 x 10^{-18}	-7.166 x 10^{-36}	110.45 x 10^{-9}	2.75 x 10^{-17}	74

Figure SI 4: Sketch of the equivalent point probe two-dipole model describing the tip - MNP interaction.

Sup. Mat. 5: Determination of the magnetic moments of oligomers

Firstly, from the fitting parameter t , we find the virtual location of the magnetic moment of the tip and its values by extrapolating the linear fit from figure 2. Secondly from parameter a based on relation (4) we can determine the magnetic moment of the cluster and subsequently comparing it with its theoretical value.

Table SI 2: MNPs clusters; fitting parameters of $\Delta\varphi = f(z)$ curves within dipole-dipole model; experimental tip's magnetic moment and its virtual location within the tip volume; experimental and theoretical clusters magnetic moments and recovery percentage.

Clusters of MNPs	Parameter a from fit (m^5)	Parameter t from fit (m)	Virtual location within the tip's volume (nm)	Experimental magnetic moment of the tip (Am^2)	Experimental magnetic moment of clusters (Am^2)	Theoretical magnetic moment of clusters (Am^2)	Recovery percentage $(\%)$
D1	-6.625×10^{-36}	110.82×10^{-9}	79	2.95×10^{-17}	6.91×10^{-18}	10.1×10^{-18}	68.5
D2	-7.896×10^{-36}	114.15×10^{-9}	82	3.16×10^{-17}	7.69×10^{-18}	10.19×10^{-18}	75.5
Tr1	-22.92×10^{-36}	136.46×10^{-9}	102	4.61×10^{-17}	14.76×10^{-18}	16.57×10^{-18}	90
Tr2	-16.65×10^{-36}	131.08×10^{-9}	98	4.32×10^{-17}	11.85×10^{-18}	13.86×10^{-18}	85.5
Tr3	-11.85×10^{-36}	124.37×10^{-9}	93	3.96×10^{-17}	9.2×10^{-18}	11.48×10^{-18}	80
Tr4	-7.51×10^{-36}	112.84×10^{-9}	81	3.09×10^{-17}	7.47×10^{-18}	11.27×10^{-18}	66
Tr5	-12.27×10^{-36}	118.64×10^{-9}	86	3.45×10^{-17}	10.94×10^{-18}	15.79×10^{-18}	70
Te	-16.31×10^{-36}	141.12×10^{-9}	96	4.17×10^{-17}	12.01×10^{-18}	18.96×10^{-18}	64
Pe	-27.06×10^{-36}	148.92×10^{-9}	110	5.18×10^{-17}	16.03×10^{-18}	24.1×10^{-18}	67

Figure SI5: Topographic AFM images (400 x 150 nm^2) of the six spherical MNPs and their corresponding height profiles taced across them as indicated by the green lines.

Figure SI6: Topographic AFM images of oligmer D1 (350 x 150 nm^2) and cluster D2 ((350 x 200 nm^2) and their corresponding height profiles taced across them as indicated by the green lines.

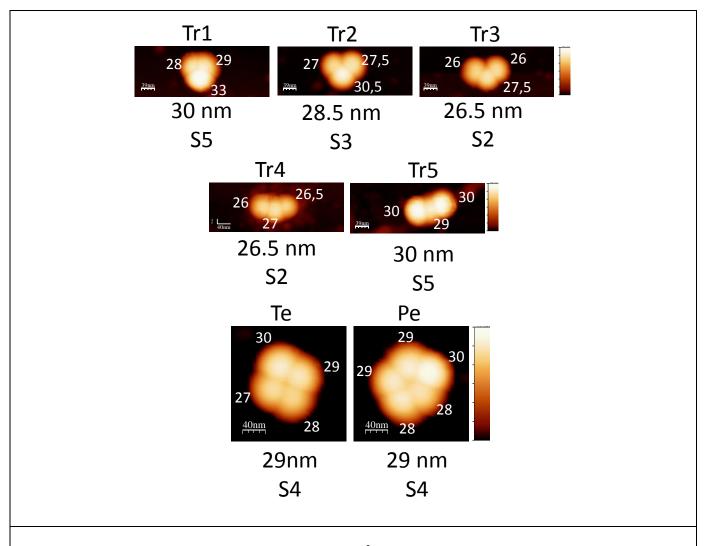**Figure SI7**: Topographic AFM images (400 x 150 nm^2) of the five trimeric clusters, one tetramer (200 x 200 nm^2) and one pentamer (200 x 200 nm^2). The diameters of the MNP composing the - clusters are indicated on each topographic image in white (the unit is nanometer) whereas their mean diameter is indicated below each topographic image. The corresponding monomer of each - cluster is indicated as well.
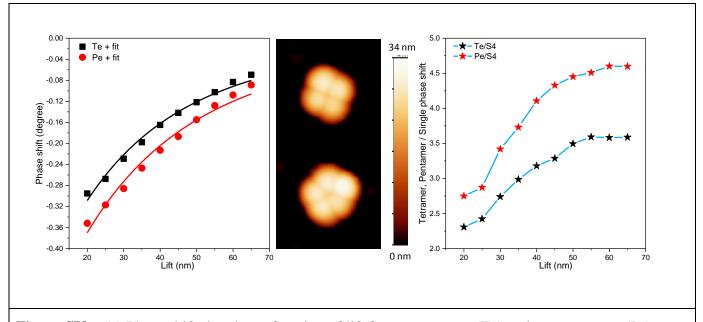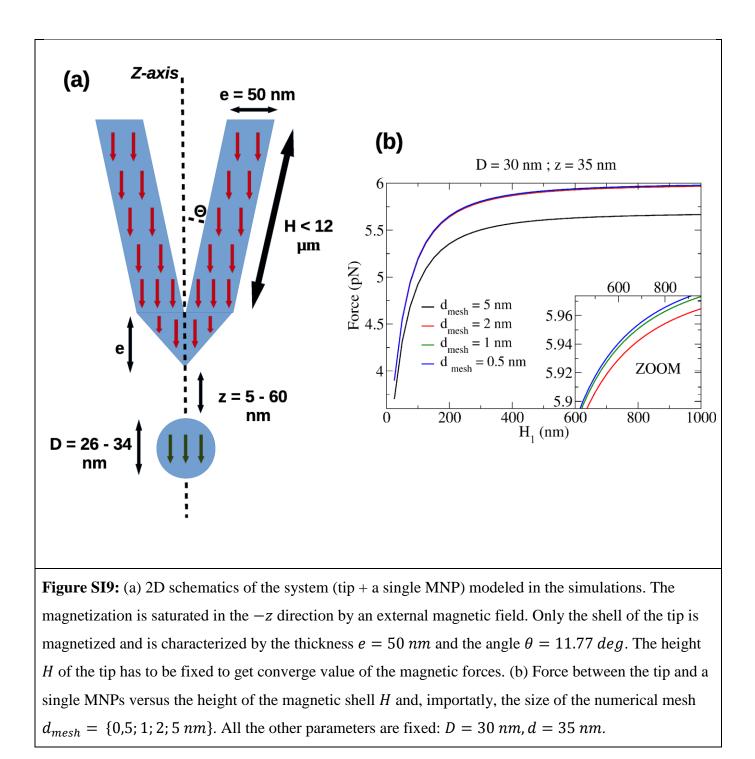
Figure SI8: . (a) Phase shift signal as a function of lift for one tetramer (Te) and one pentamer (Pe) along with their corresponding two-dipole fits (solid lines). The insets represent AFM topographic images of Te and Pe (250 x 250 nm²) a along with the scketch of a square and of a pentagon to show the spatiall arrangement of the MNPs (b) Phase shifts for the tetramer and pentamer divided by the phase shift of a single MNP, as a function of tip lift.

Sup. Mat. 6: Theoretical modeling of tip-single MNPs geometry

The real geometry of the tip interacting with a single MNPs used in theoretical simulations is sketched in the Fig. SI9. It is considered that the tip has the geometry of a cone, where only a shell of $e = 50\ nm$ around the cone is magnetic. The basis of the cone is a disk with a radius $L = 2.5\ \mu m$ and the height of the cone is $H = 12\ \mu m$. The angle $\theta = \tan{(H/L)}^{-1}$ is related to the size of the tip and is equal to 11.77 deg. Typically the different parameters that vary are: D – the diameter of the magnetic nanoparticle and z - the distance between the tip and the MNPs. The height of the tip H has to be fixed to get a convergence of the force. The full system is cut into small magnetic elements with a characteristic size d_{mesh}. The elementary force between two elementary magnetic elements with respective magnetic moments $\overrightarrow{M_1}$ and $\overrightarrow{M_2}$ and connected together by the vector $\vec{r}$, reads as seen in Eq 2 in the main text.

In our model, we assume that the magnetization densities of the MNPs and the tip are fixed and saturated in the $-z$ direction: $\overrightarrow{m_{MNPs}} = -3.85\ x\ 10^5\ \vec{e_z}\ [\frac{A}{m^2}]$ and $\overrightarrow{m_{Tip}} = -3.50\ x\ 10^5\ \vec{e_z}\ [\frac{A}{m^2}]$. Then, the total magnetic force is obtain by integrating the elementary force over the all system, resulting in Eq. 3 from the main text.

The spatial integration variables: $\vec{r}'$and $\vec{r}''$ in Eq 3 from the manuscript run, respectively, over the MNPs and the tip. The integration can be done analytically for some simple cases such as two spheres, but for more complex geometries it has to be done numerically. In all the study, we will only focus on the force along the z direction, $F_z \equiv F$. The other components are often non zero but we assume that they do not contribute to the phase shift measured in the experiments. The computed force is sensible to the size of the mesh, d_{mesh}, but also to the height of the tip, H. In figure SI9, it is plotted the magnetic force exerted on the tip by a single MNPs varying both d_{mesh} and H. It can be seen that in order to converge the magnetic force, a mesh lower than 2 nm it is necessary as well as a large value for the tip height $H > 500\ nm$. Therefore, the following values: $H = 500\ nm$ and $d_{mesh} = 2\ nm$ are used in the theoretical simulations to calculate the magnetic forces.

Figure SI9: (a) 2D schematics of the system (tip + a single MNP) modeled in the simulations. The magnetization is saturated in the $-z$ direction by an external magnetic field. Only the shell of the tip is magnetized and is characterized by the thickness $e = 50\ nm$ and the angle $\theta = 11.77\ deg$. The height H of the tip has to be fixed to get converge value of the magnetic forces. (b) Force between the tip and a single MNPs versus the height of the magnetic shell H and, importatly, the size of the numerical mesh $d_{mesh} = \{0,5; 1; 2; 5\ nm\}$. All the other parameters are fixed: $D = 30\ nm, d = 35\ nm$.

Sup. Mat. 7: Calculation of trimer/single phase shift ratio with the two-dipole model

In the case of the compact cluster ($\theta = \pi/3$) the magnetic dipoles are located at the coordinates $(0; R; 0)$, $(R; -R(1 - 2\sqrt{3}); 0)$, $(-R; -R(1 - 2\sqrt{3}); 0)$, while the tip at $(0; 0; d + R)$.

In the case of the linear clusters ($\theta = \pi$) the magnetic dipoles are located at the coordinates $(0; -2R; 0)$, $(0; 0; 0)$, $(2R; 0; 0)$, while the tip at $(0; 0; d + R)$.

In both cases, R represent the MNPs radius. The magnetic dipoles representing the MNPs are all equal $(0; 0; M_{MNPs})$ whereas the magnetic dipole representing the tip is given by $(0; 0; M_{Tip})$.

By using the equation (5), the analytical expressions for the trimer/single phase shift ratio can be derived as follow:

$$\frac{\phi(Trimer)}{\phi(Single)} = \frac{3x^5 \left(x^4 - 4x^2 + \frac{2}{3}\right)}{\left(\frac{4}{3} + x^2\right)^{\frac{9}{2}}} \qquad \left(\theta = \frac{\pi}{3}\right) \qquad (5)$$

$$\frac{\phi(Trimer)}{\phi(Single)} = 1 + \frac{2x^5 (x^4 - 12x^2 + 6)}{(4 + x^2)^{9/2}} \qquad (\theta = \pi) \qquad (6)$$

where $x = d/R$.

References:

[1] Sun, S.; Zeng, H., Size-Controlled Synthesis of Magnetite Nanoparticles, *J. Am. Chem. Soc.*, **2002**, *124*, 8204–8205.

[2] Sasaki, S., Radial Distribution of Electron Density in Magnetite, Fe_3O_4. *Acta Crystallogr. Sect. B Struct. Sci.*, **1997**, *53*, 762–766.

[3] Patterson, A. L., The Scherrer formula for X-ray particle size determination, *Phys. Rev.*, **1939**, *56*, 978–982.